Ion Dose Uniformity for Planar Sample Plasma Immersion Ion Implantation

Dixon Tat-Kun Kwok, Paul K. Chu, *Member, IEEE,* and Chung Chan, *Fellow, IEEE*

***Abstract*—In spite of recent progress on plasma immersion ion implantation (PIII) in semiconductor processing, for example, formation of silicon on insulators and shallow junctions, ion dose, and energy uniformity remains a major concern. We have recently discovered that the sample stage (chuck) design can impact ion uniformity significantly. Using a theoretical model, we have investigated three different chuck designs and conclude that insulators on the stage can alter the adjacent electric field and ion trajectories. Even though the conventional stage design incorporating a quartz shroud reduces the load on the power supply and contamination, it yields ion dose and energy nonuniformity unacceptable to the semiconductor industry. Thus, for semiconductor applications, the stage should be made of a conductor, preferably silicon or silicon coated materials and free of quartz.**

***Index Terms*—Chuck design, ion dose uniformity, plasma immersion ion implantation, semiconductor processing.**

I. Introduction

PLASMA immersion ion implantation (PIII) is a burgeoning technique for semiconductor processing due to its high dose rate and simple instrumentation [1]–[4]. In PIII, the wafers are surrounded by high-density plasma and pulse biased to a high negative potential relative to the chamber wall. Ions generated in the plasma shroud are accelerated across the sheath formed around the samples and implanted into the surface of the targets. Since the entire wafer is implanted simultaneously, the implantation time is much shorter than that of conventional beamline techniques, and the time advantage is more substantial for larger wafer size such as 300 mm. It has thus been used to form shallow junctions [5]–[8], synthesize silicon-on-insulator (SOI) structures [9]–[17], process flat panel display materials [18], and so on.

Most PIII instruments consist of a stainless steel cylindrical vacuum chamber with internal liners made of aluminum or compatible materials to minimize contamination to the specimens. The sample holder (chuck) is typically made of stainless steel (for high temperature and general applications) or aluminum (for low temperature processing) and is typically located in the center of the chamber. The stage is directly connected to a negative high voltage pulse generator/modulator and the wafer is placed on top of the chuck [Fig. 1(a)]. Because of the absence of ion transport optics, ions will be implanted to both the sample and chuck, and the large current demands a big power supply/modulator. In order to avoid contamination from the chuck and to reduce the current drawn to the wafer chuck, an insulator like a quartz tube or quartz plate is usually used to cover up the exposed part of the wafer holder as depicted in Fig. 1(b) and (c). These chuck designs are adequate for metallurgical applications in which minor ion dose and energy fluctuations are tolerable. However, we have recently observed that the insulator shroud on the chuck becomes charged during PIII and the electric field alters the ion trajectories [19]. It causes nonuniformity in both the ion dose and energy and the results are unacceptable to semiconductor processing.

When a negative high voltage pulse is applied to a target immersed in plasma, electrons are expelled from the region near the target. The ions are relatively motionless because of their heavier mass, leaving a region of nearly pure ion space charge. That is, an initial ion-matrix sheath is formed [20]. Subsequently, ions are accelerated toward the target as they fall through the ion-matrix sheath. On a longer time scale, the decreasing ion density inside the sheath region due to the ion collection on the target causes the dynamic sheath edge to expand in order to maintain the sheath potential. Ultimately, the ion and electron density profiles relax to establish a steady-state Child–Langmuir sheath. Therefore, the ion motion is strongly dependent on the dynamic sheath and its expansion, which consequently depends on the shape of the negative biased target. We will expect that the sheath will evenly form around the cylindrical wafer holder as shown in Fig. 1(a). However, as shown in Fig. 1(b) and (c), since part of the wafer holder is covered by an insulating quartz shroud, the shape of the sheath will be quite different from that in Fig. 1(a).

In this paper, we present the ion motions and sheath expansion for three different holder configurations:

I) plain wafer chuck [Fig. 1(a)];
II) wafer chuck surrounded by quartz tube [Fig. 1(b)];
III) wafer chuck surrounded by quartz tube and covered by quartz plate [Fig. 1(c)].

The potential sheath, ion density distribution, and ion velocity vector inside the chamber at different time are investigated. The lateral variation of the ion implantation dose as well as ion impact angle is also presented.

II. Kinetic Model

We make two assumptions for the ions. First, the ions are assumed to be noncollisional and cold. Second, they acquire

Manuscript received February 10, 1998. This work was supported by City University of Hong Kong Strategic Grant 7000730 and Hong Kong RGC Earmarked Grants 9040220 and 9040332.

D. T.-K. Kwok and P. K. Chu are with the Department of Physics and Materials Science, City University of Hong Kong, Kowloon, Hong Kong (e-mail: paul.chu@cityu.edu.hk).

C. Chan is with the Department of Electrical and Computer Engineering, Northeastern University, Boston, MA 02115 USA.

Publisher Item Identifier S 0093-3813(98)09644-1.

0093–3813/98$10.00 © 1998 IEEE

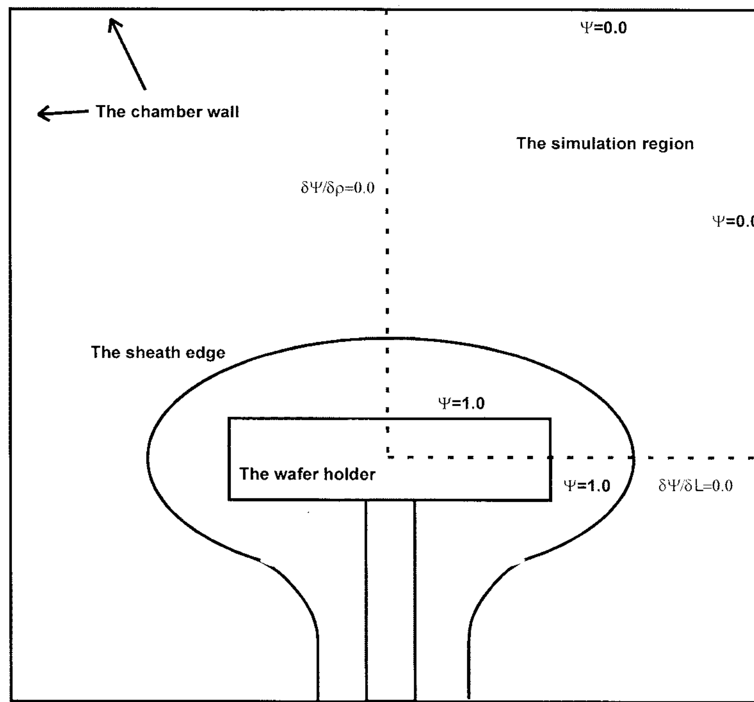

(a)

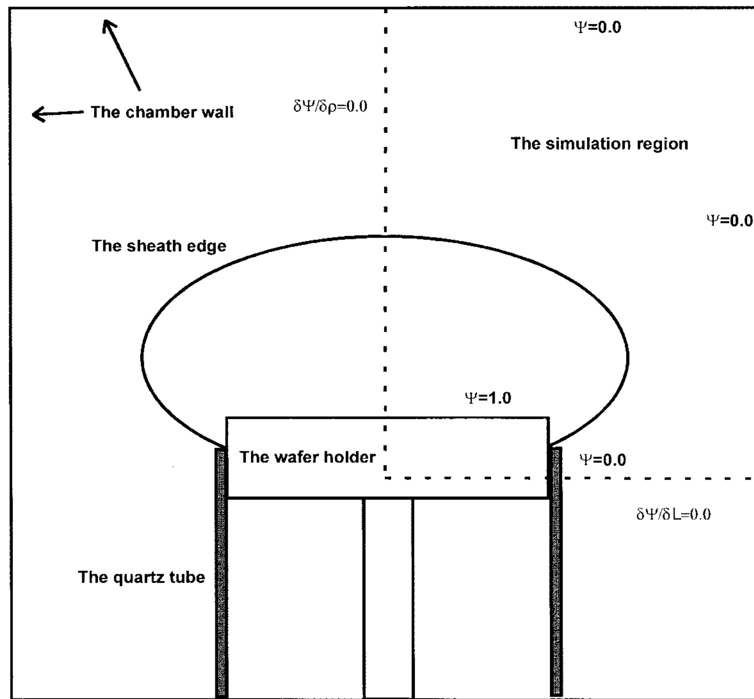

(b)

Fig. 1. (a) Schematic diagram of the PIII chamber with a plain wafer holder. The simulation region is surrounded by the dotted lines. (b) Schematic diagram of the PIII chamber with the wafer holder surrounded by a quartz shroud. The surface of the quartz tube is grounded.

directed motion only by the electric field. The electrons are assumed to be in thermal equilibrium, so that the electron density n_e is given by the Bolzmann's relationship

$$n_e = n_o \exp\left(\frac{e\phi}{kT_e}\right) \tag{1}$$

where n_o is the initial ion density, k is the Boltzmann's constant, and T_e is the electron temperature. Thus, in our model, we only need to follow the ion dynamics.

Poisson's equation will relate the potential ϕ to the electron density n_e and ion density n_i as follows:

$$\nabla^2\phi = -\frac{e}{\varepsilon_o}(n_i - n_e) \tag{2}$$

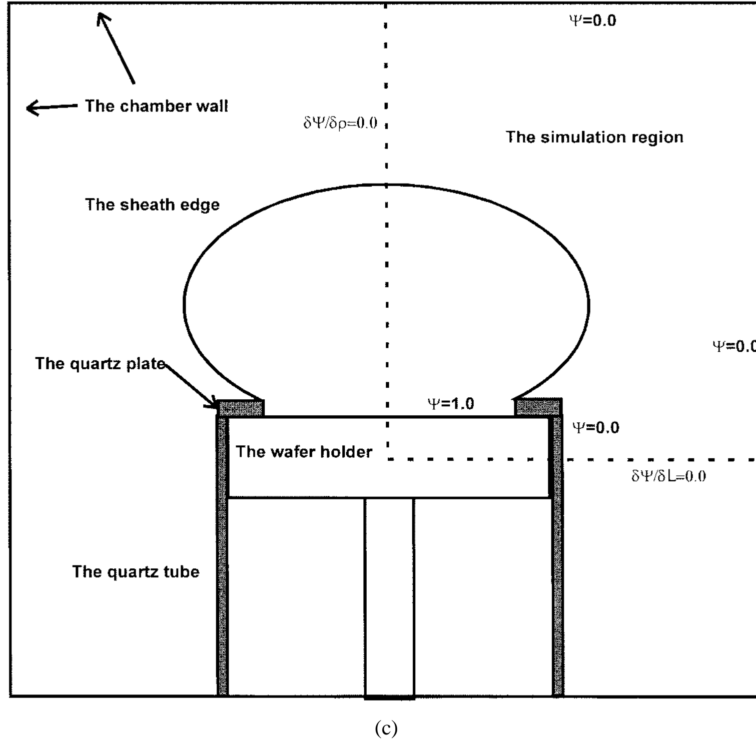

(c)

Fig. 1. *(Continued.)* (c) Schematic diagram of the PIII chamber with the wafer holder surrounded by a quartz shroud and partially covered by a quartz plate. The expansion of the presheath is restricted by the quartz plate.

where ε_o is the permittivity in free space and e is the electron charge. The motions of the ion are governed by Newton's equations of motion

$$\boldsymbol{F} = M\boldsymbol{a} \tag{3}$$

$$\boldsymbol{V}(f) = \boldsymbol{V}(I) + \boldsymbol{a}t \tag{4}$$

$$\Delta\boldsymbol{d} = \boldsymbol{V}(I) + \tfrac{1}{2}\boldsymbol{a}t^2 \tag{5}$$

where $\boldsymbol{F}$ is the force applied on the particle (ion). In this case,

$$\boldsymbol{F} = -q\nabla\phi \tag{6}$$

q is the charge of the particle (ion), M is the mass of the particle (ion), $\boldsymbol{a}$ is the acceleration, $\boldsymbol{V}(f)$ and $\boldsymbol{V}(I)$ are the final and initial velocities, and $\boldsymbol{\Delta}d$ is the distance traversed by the ion in time t.

Due to the symmetry in cylindrical coordinates, (1), (2), (4), and (5) become

$$\frac{\partial^2\phi}{\partial r^2} + \frac{1}{r}\frac{\partial\phi}{\partial r} + \frac{\partial^2\phi}{\partial z^2} = -\frac{e}{\varepsilon_o}\left[n_i - n_o\exp\left(\frac{e\phi}{kT_e}\right)\right] \tag{7}$$

$$v_i^r(f) = v_i^r(I) - \frac{q}{M}\frac{\partial\phi}{\partial r}t \tag{8a}$$

$$v_i^z(f) = v_i^z(I) - \frac{q}{M}\frac{\partial\phi}{\partial z}t \tag{8b}$$

$$\Delta r = v_i^r(I)t - \frac{1}{2}\frac{q}{M}\frac{\partial\phi}{\partial r}t^2 \tag{9a}$$

$$\Delta z = v_i^z(I)t - \frac{1}{2}\frac{q}{M}\frac{\partial\phi}{\partial z}t^2. \tag{9b}$$

The plasma quantities can be made dimensionless by normalization

$$\rho = \frac{r}{D},\quad L = \frac{z}{D},\quad T = t\omega_{pi},\quad \Psi = \frac{\phi}{\phi_p}$$

$$N = \frac{n_i}{n_o},\quad V^L = \frac{v_i^z}{v_{\max}},\quad \text{and}\quad V^\rho = \frac{v_i^r}{v_{\max}}$$

where $D = \sqrt{-4\varepsilon_o\phi_p/en_o}$ is the ion-matrix overlap length, $\omega_{pi} = \sqrt{n_o e^2/\varepsilon_o M}$ is the ion plasma frequency, and $v_{\max} = \sqrt{-2e\phi_p/M}$ is the velocity the ion would have if it fell through a potential drop ϕ_p. After normalization, (7)–(9) are simplified

$$\frac{\partial^2\Psi}{\partial\rho^2} + \frac{1}{\rho}\frac{\partial\Psi}{\partial\rho} + \frac{\partial^2\Psi}{\partial L^2} = 4\left(N - e^{-c\Psi}\right) \tag{10}$$

where $c = e|\phi_p|/kT_e$

$$V^\rho(f) = V^\rho(I) + \frac{1}{\sqrt{8}}\frac{\partial\Psi}{\partial\rho}T \tag{11a}$$

$$V^L(f) = V^L(I) + \frac{1}{\sqrt{8}}\frac{\partial\Psi}{\partial L}T \tag{11b}$$

$$\Delta\rho = \frac{1}{\sqrt{2}}V^\rho(I)T + \frac{1}{8}\frac{\partial\Psi}{\partial\rho}T^2 \tag{12a}$$

$$\Delta L = \frac{1}{\sqrt{2}}V^L(I)T + \frac{1}{8}\frac{\partial\Psi}{\partial L}T^2. \tag{12b}$$

III. Numerical Simulation

As shown in Fig. 1(a)–(c) which depict the vertical cross section of the chamber and wafer chuck, the center line will symmetrically divide the chamber into two equal halves. The midplane of the wafer chuck ($L = 0$) is another symmetry

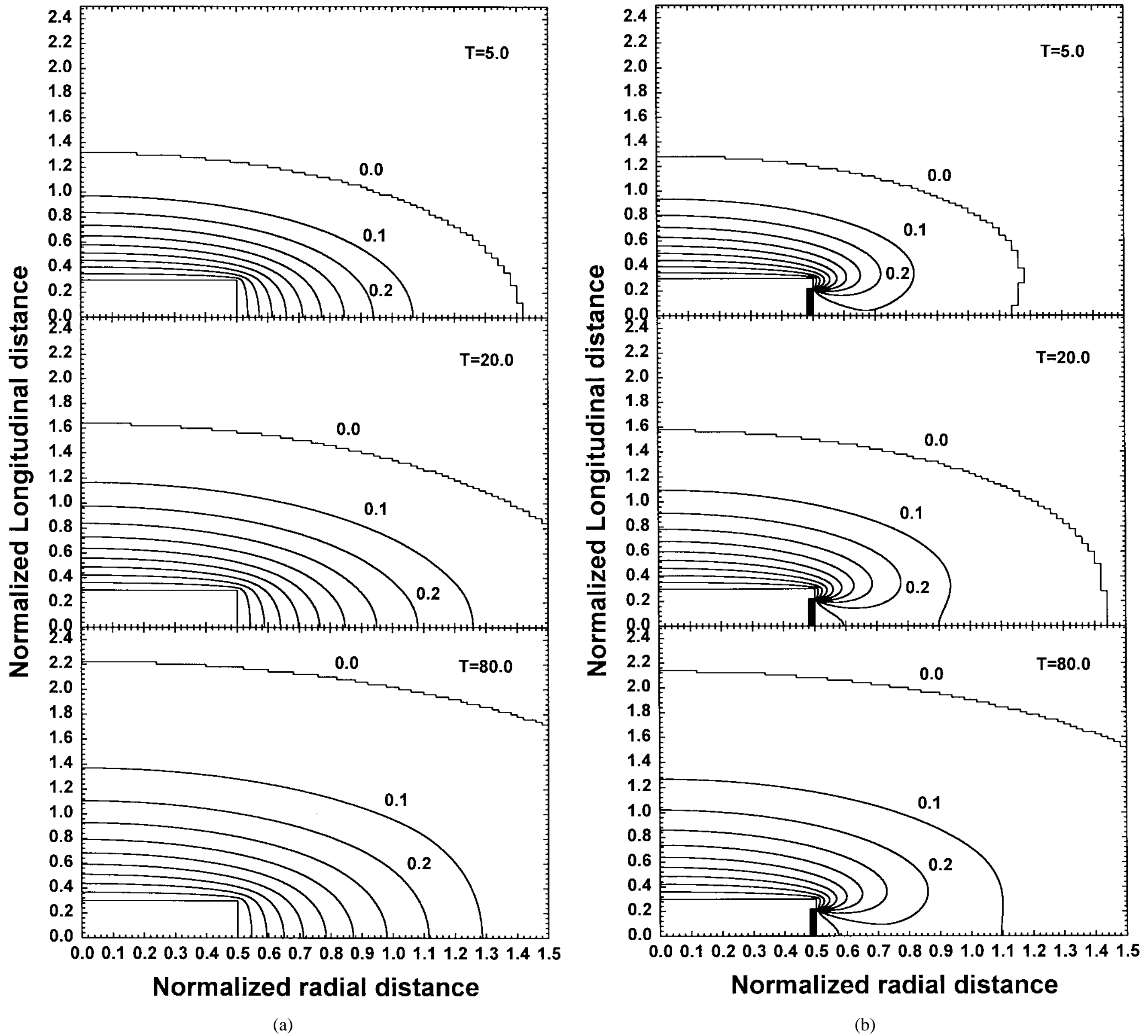

Fig. 2. (a) Evolution of the normalized potential contour lines for case 1 [Fig. 1(a)]. The expansion of potential contour lines follow the rectangular shape of the wafer holder. (b) Evolution of the normalized potential contour lines for case 2 [Fig. 1(b)]. A regional electric field forms between the wafer holder and quartz shroud.

plane and only a quarter of the vertical cross section of the wafer chuck is thus required in our simulation. The simulation regions of the three different cases, i.e., 1) without quartz covers, 2) quartz tube, and 3) quartz tube plus quartz plate, are demarcated by dotted lines in Fig. 1(a)–(c).

The top and right-hand side boundaries of the simulation regions are the chamber walls. Therefore, at these boundaries, $\Psi = 0.0$. At the left symmetry boundary $\partial\Psi/\partial\rho = 0.0$, whereas at the bottom symmetry boundary $\partial\Psi/\partial L = 0.0$. The rise time of the applied voltage is set to zero. On the wafer chuck surface $\Psi = 1.0$ and $\Psi = 0.0$ on the surface of the quartz plate and quartz tube. Initially, the ions are evenly distributed among the simulation region.

We adopt the finite difference method to simulate (10)–(12). The simulation process is divided into tiny square meshes with size $h \times h$. $\Psi_{i,j,k}$, $N_{i,j,k}$, $V^{\rho}_{i,j,k}$, and $V^{L}_{i,j,k}$ represent the normalized potential, ion density, radial ion velocity, and longitudinal ion velocity at position $\rho = ih$, $L = jh$, and at time kf, respectively, f is the time step used in the simulation, and i, j, and k are positive integers. To approximate the normalized potential Ψ in (10), we use the centered difference formulas

$$\frac{\partial^2\Psi}{\partial\rho^2} \approx \frac{\Psi_{i+1,j,k} + \Psi_{i-1,j,k} - 2\Psi_{i,j,k}}{h^2}$$

$$\frac{\partial^2\Psi}{\partial L^2} \approx \frac{\Psi_{i,j+1,k} + \Psi_{i,j-1,k} - 2\Psi_{i,j,k}}{h^2}$$

$$\frac{\partial\Psi}{\partial\rho} \approx \frac{\Psi_{i+1,j,k} - \Psi_{i-1,j,k}}{2h}$$

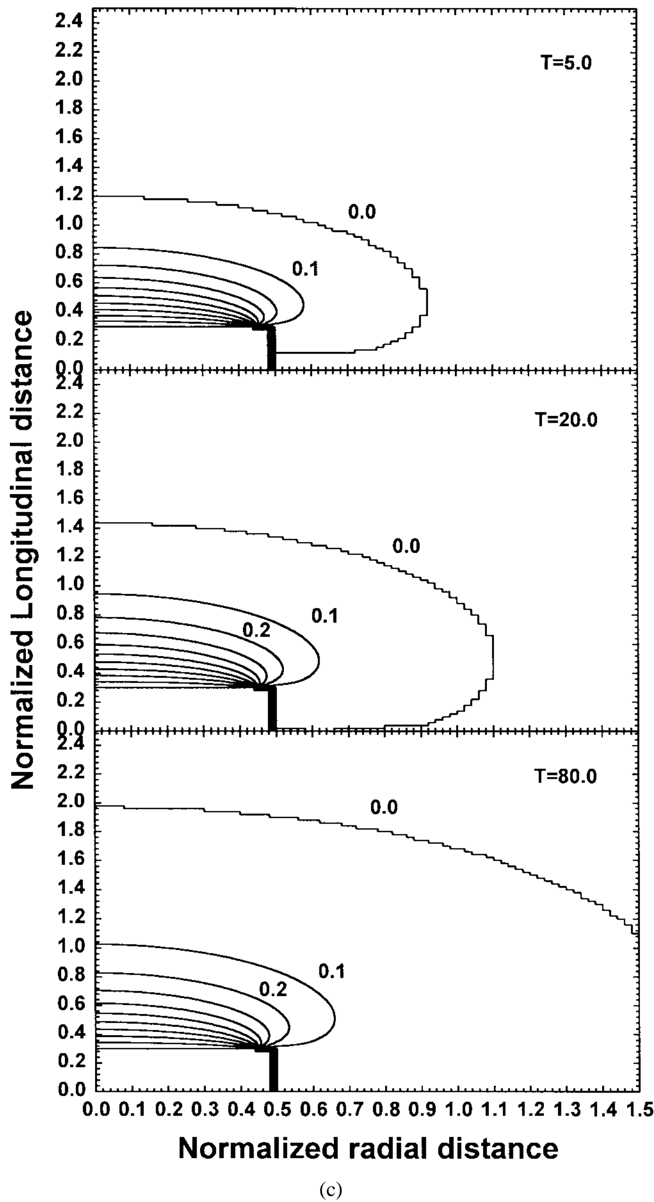

(c)

Fig. 2. *(Continued.)* (c) Evolution of the normalized potential contour lines for case 3 [Fig. 1(c)]. A regional electric field forms between the wafer holder and quartz plate.

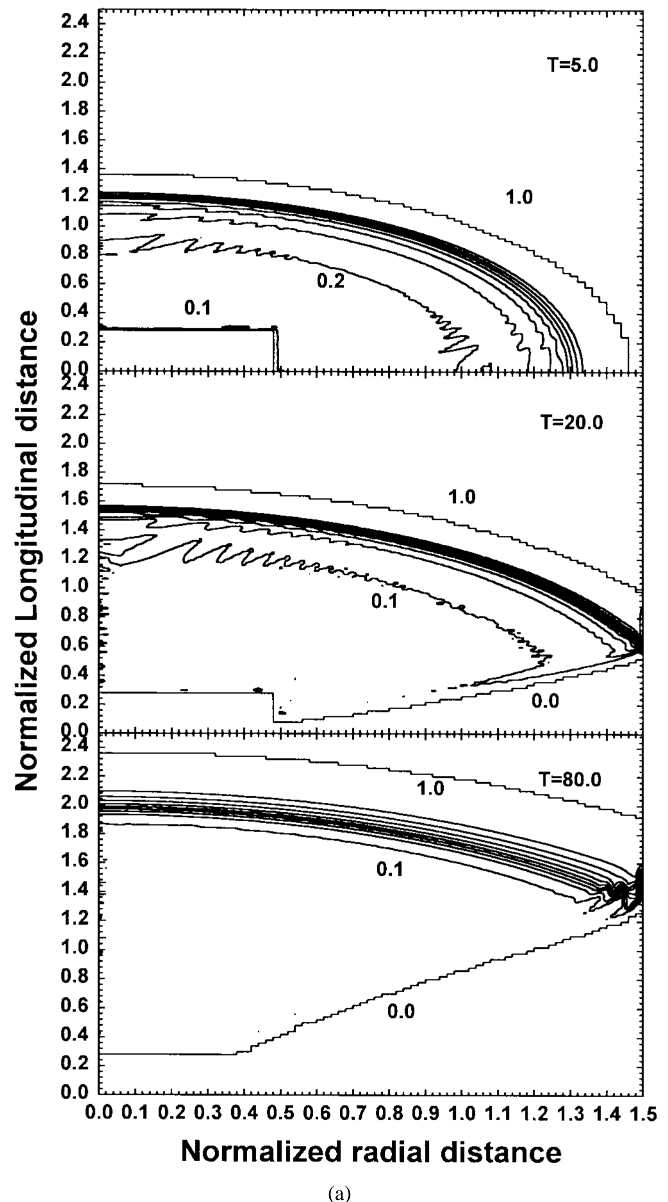

(a)

Fig. 3. (a) Evolution of the normalized ion density contour lines for case 1 [Fig. 1(a)]. A zero ion density contour line forms and moving to the top surface of the wafer holder.

and

$$\frac{\partial \Psi}{\partial L} \approx \frac{\Psi_{i,\,j+1,\,k} - \Psi_{i,\,j-1,\,k}}{2h}.$$

However, along the surfaces of the wafer holder/quartz plate, we use the approximations

$$\frac{\partial \Psi}{\partial L} \approx \frac{\Psi_{i,\,j+1,\,k} - \Psi_{i,\,j,\,k}}{h} \text{ along the vertical direction}$$

and

$$\frac{\partial \Psi}{\partial \rho} \approx \frac{\Psi_{i+1,\,j,\,k} - \Psi_{i,\,j,\,k}}{h} \text{ along the horizontal direction.}$$

Equation (10) is solved via numerical iteration by first letting Φ be an initial solution and linearizing (10) about this value using the relationship

$$\begin{aligned} \exp(-c\Psi) &= \exp(-c\Phi)\,\exp(-c(\Psi - \Phi)) \\ &\approx \exp(-c\Phi)(1 - c\Psi + c\Phi). \end{aligned}$$

Then we plug in Φ from Ψ calculated from the previous time step, solve (10) to obtain a new Ψ, set Φ equal to this new Ψ, and iterate until the process converges.

The position and velocity of each particle (ion) at a particular time step are defined by (11) and (12). $\partial\Psi/\partial\rho$ and $\partial\Psi/\partial L$ are estimated according to the particle (ion) position in space. After the new position and velocity of all the particles (ions) are updated, they will be weighted to the four corners of the mesh containing the particle (ion). Finally, the normalized ion density $N_{i,\,j,\,k}$, radial velocity $V^{\rho}_{i,\,j,\,k}$, and longitudinal velocity

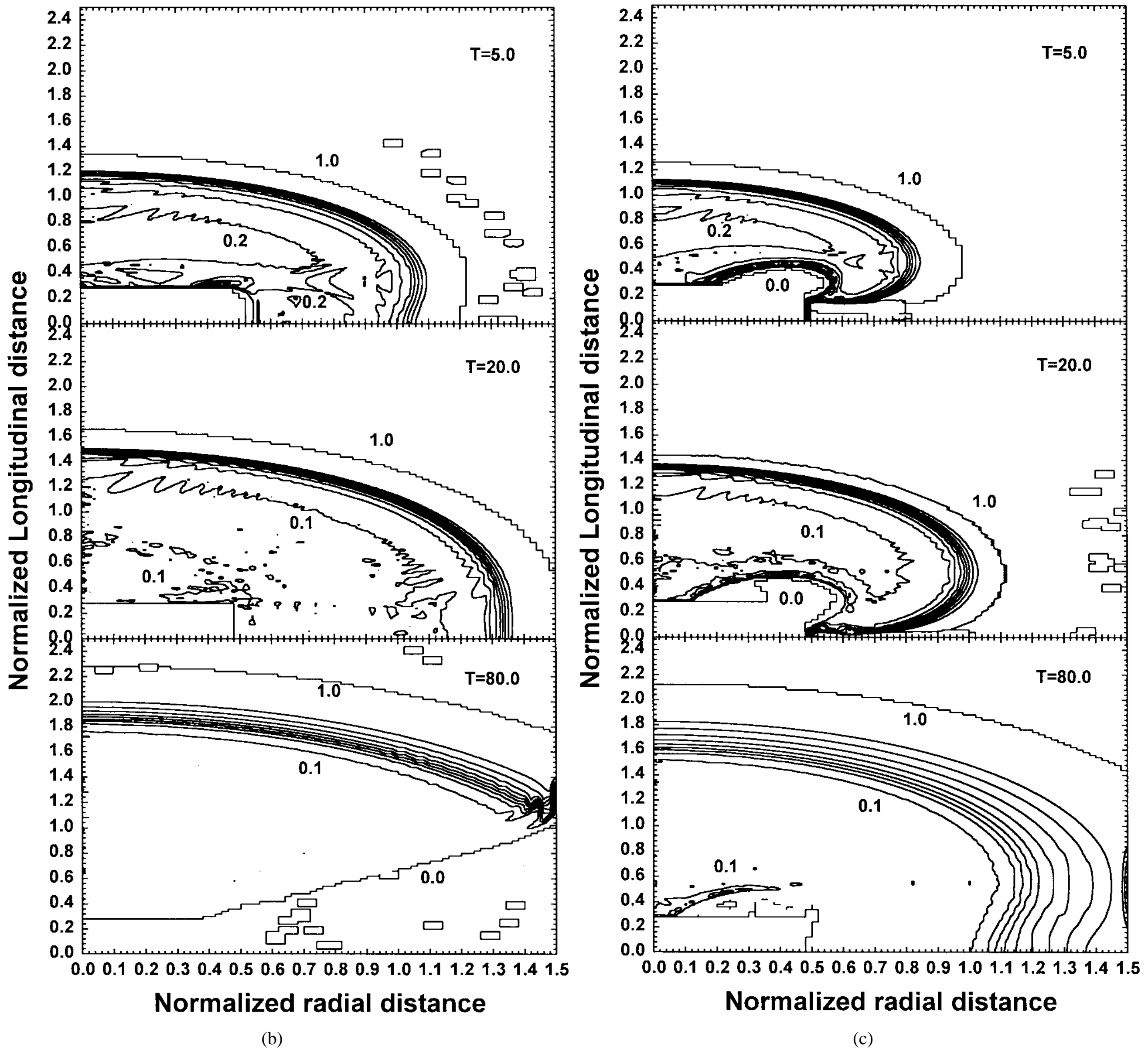

Fig. 3. *(Continued.)* (b) Evolution of the normalized ion density contour lines for case 2 [Fig. 1(b)]. The tiny squares are produced by a few ions escaping to that area. (c) Evolution of the normalized ion density contour lines for case 3 [Fig. 1(c)]. A small empty hole forms on the surface of the wafer holder.

$V^L_{i,j,k}$ are obtained within the simulation region and ready for the next time step of iteration.

When the particle (ion) hits the wafer chuck, it will be removed. The dose surrounding the bombardment area will be automatically accumulated. If the particle (ion) crosses the boundary $\rho = 0$ or $L = 0$, it is assumed that another particle from the other side with reverse ion velocity V^ρ or V^L will cross the boundary refilling the lost particle.

IV. Results and Discussions

To make a more general discussion, all the variables are expressed in dimensionless normalized units. The following physical configuration is modeled: radius of the wafer holder = 0.5 D, thickness (half) of the wafer holder = 0.3 D, radius of the chamber = 1.5 D (three times the radius of the wafer chuck), height of the chamber measured from the top of the wafer holder = 2.5 D, zero rise time for the applied potential $c = 3750$, $1\phi_p 1 = 15\ 000\ V$, and $T_e = 4eV$. The simulation parameters are: grid spacing $h = 0.02$ D and time step $k = 0.002T_{pi}$ where $T_{pi} = 1/\omega_{pi}$. A total of $125 \times 75 = 9375 - 25 \times 15 = 375$ cells are formed in the simulation region, and 100 particles (ions) are initially uniformly placed in each cell (900 000 initial particles). The simulation is terminated at $t = 100T_{pi}$. In case one, the wafer chuck is exposed and the potential along the vertical and horizontal surfaces is 1.0. In the second case, the wafer chuck is surrounded by a quartz shroud of height 0.2 D, and the potential on the quartz tube is 0.0. We assume that the thickness of the quartz tube or plate is much thinner than the radius and thickness of the wafer chuck. In the third case, the wafer holder is surrounded by a quartz shroud and partly covered by a quartz plate, and the potential along the vertical

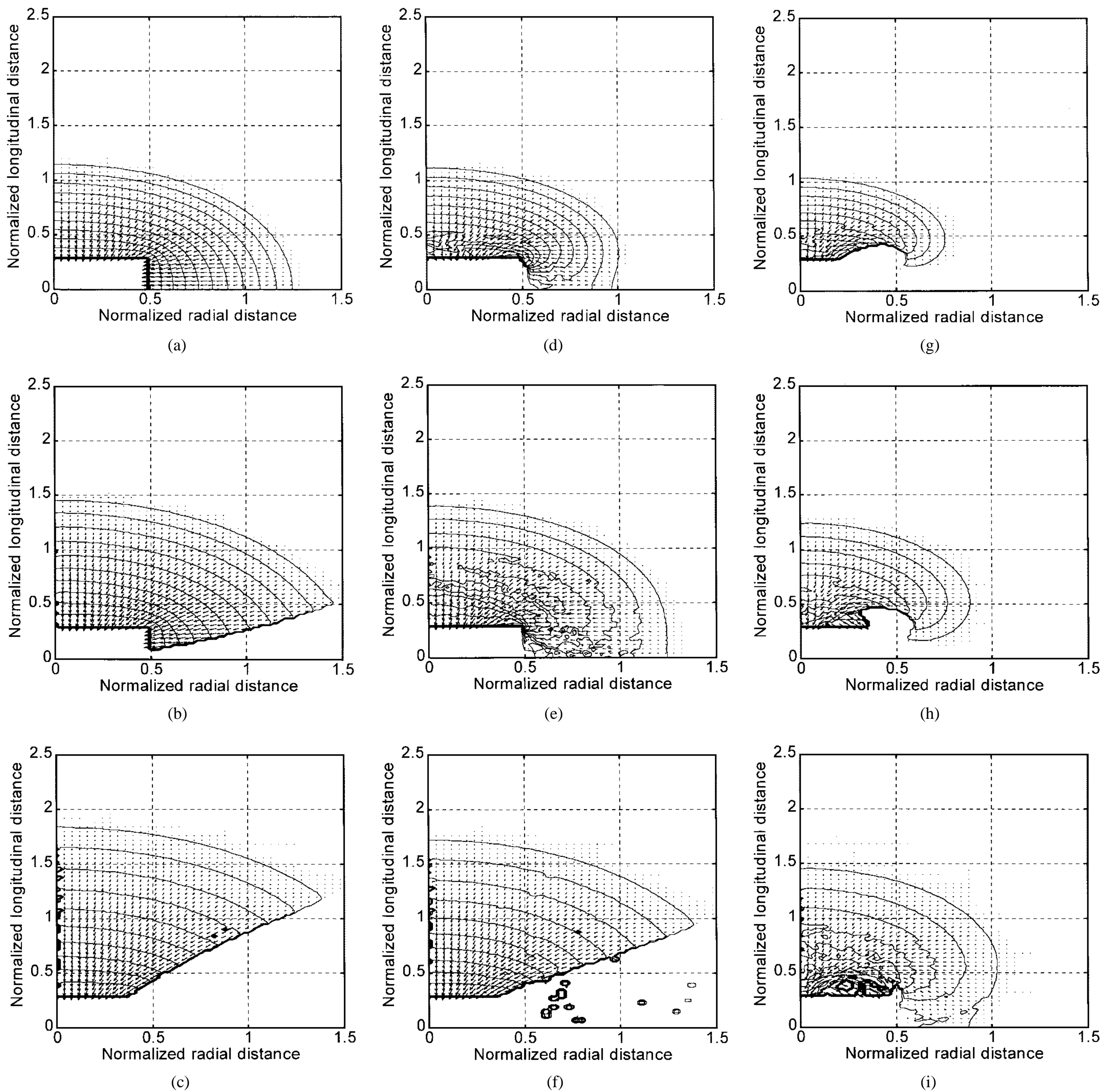

Fig. 4. Ion velocity vector at (a) $T = 5$, (b) $T = 20$, and (c) $T = 80$ for case 1 [Fig. 1(a)]. Ion velocity vector at (d) $T = 5$, (e) $T = 20$, and (f) $T = 80$ for case 2 [Fig. 1(b)]. Ion velocity vector at (g) $T = 5$, (h) $T = 20$, and (i) $T = 80$ for case 3 [Fig. 1(c)].

direction of the wafer holder is 0.0. The horizontal surfaces of the wafer chuck outside the circle of radius 0.44 D is covered by the quartz plate. Therefore, the potential of these surfaces is also 0.0.

A. Potential

The temporal evolution of the potential contour lines is shown in Fig. 2(a)–(c) for $t = 5T_{pi}, 20T_{pi}$, and $80T_{pi}$. As shown in Fig. 2(a) (case one), the potential contour lines expand evenly along the vertical and horizontal direction according to the shape of the "rectangular" wafer holder. The electron density is given by the Boltzmann's relationship in (1). When $\Psi = 0.001$, the electron density drops to $\exp(-3750 \times 0.001) = 0.0235$, i.e., less than 3%. Therefore, we can consider the zero potential contour line as the presheath edge. At $t = 5T_{pi}$, the edge of the electron sheath (presheath) almost hits the chamber wall. Later, at $t = 20T_{pi}$ and $t = 80T_{pi}$, the presheath no longer surrounds the wafer holder but forms a shield covering from the top. A strong electric field is formed along the horizontal direction between the chamber wall and the wafer holder. When the ion crosses the presheath edge, the horizontal electric field will push them toward the center.

Under the influence of the quartz tube and plate, the potential contour lines expand in a restricted way as shown in

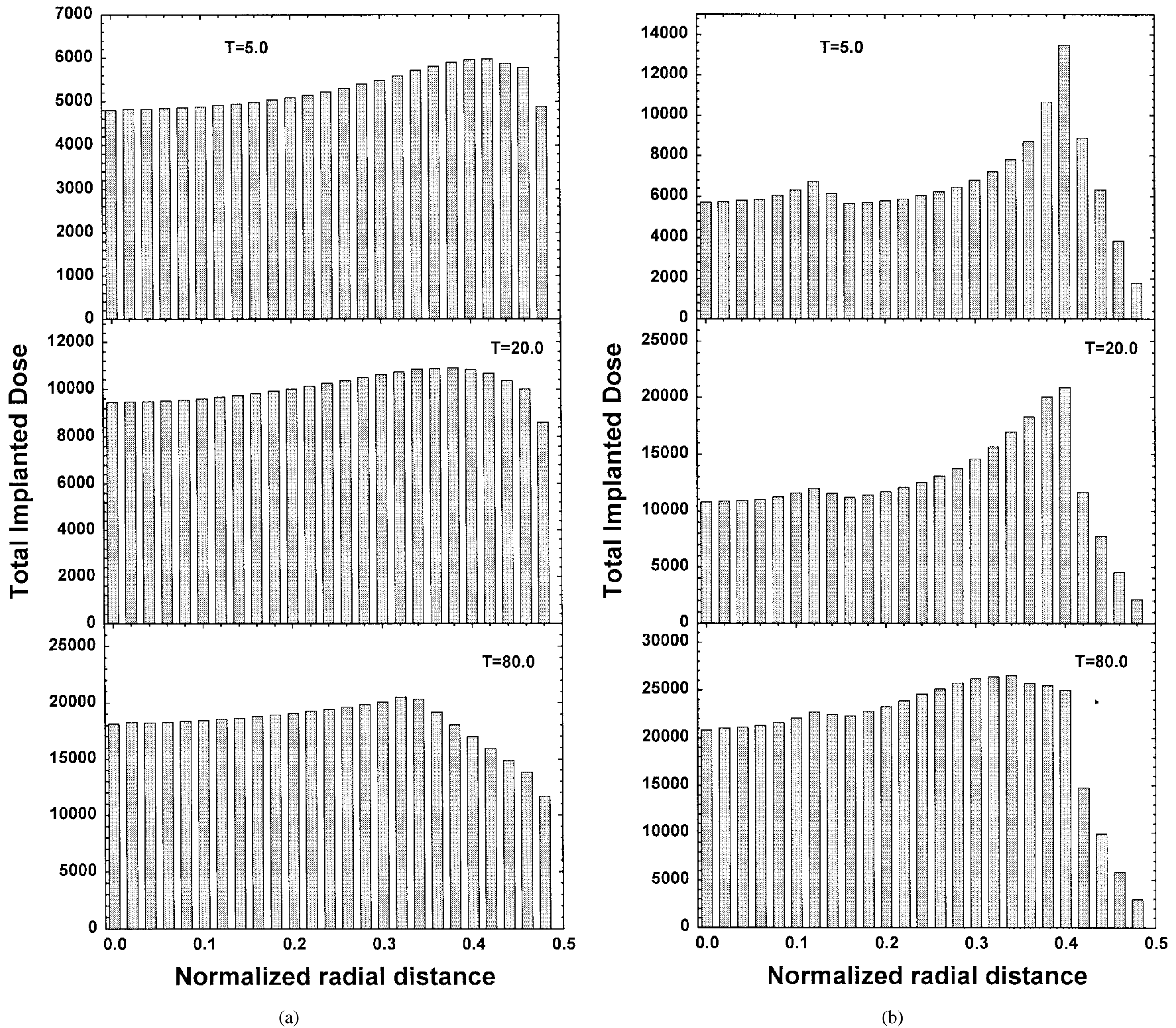

Fig. 5. (a) Variation of normalized total implantation dose along the surface of the wafer chuck at different times for case 1 [Fig. 1(a)]. Ions are implanted quite uniformly across the wafer surface. (b) Variation of normalized total implantation dose along the surface of the wafer chuck at different times for case 2 [Fig. 1(b)]. A strong peak is observed near the edge of the wafer chuck.

Fig. 2(b) (case two) and Fig. 2(c) (case three). The presheath hits the chamber wall at around $t = 20T_{pi}$ in Fig. 2(b) and at further time in Fig. 2(c). A regional electric field is formed at the border between the quartz ($\Psi = 0$) and wafer holder ($\Psi = 1.0$), i.e., at position ($\rho = 0.5$, $L = 0.2$) in Fig. 2(b), and at position ($\rho = 0.44$, $L = 0.3$) in Fig. 2(c). The regional electric field creates an anti-clockwise pulling force among the ion (see ion velocity). The difference in the position of the regional electric field between Fig. 2(b) (top right side of the corner) and Fig. 2(c) (left bottom side of the corner) is small. However, a pronounced effect on the total implantation dose is observed for the wafer placed on top of the chuck.

B. Ion Density

The temporal evolution of the ion density is exhibited in Fig. 3(a)–(c). As shown in Fig. 3(a), after the presheath hits the chamber wall, the ions begin to exhaust around the midplane. At $t = 20T_{pi}$, a zero ion density contour line is observed. Ions moving across the presheath at the top are pushed toward the center by the electric field formed between the chamber wall ($\Psi = 0$) and the wafer chuck ($\Psi = 1.0$). The zero contour line moves to the top of the wafer holder at $t = 80T_{pi}$. Therefore, at $t > 80T_{pi}$, only part of the wafer is implanted. The implanted area became smaller and smaller at latter times. The evolution of the ion density for case two depicted in Fig. 3(b) is similar to that shown in Fig. 3(a). However, under the influence of the regional electric field formed on the left bottom part of the corner, the ions are pushed toward the top right part of the corner at $t = 5T_{pi}$ and $t = 20T_{pi}$. The zero ion density contour line is formed after $t = 20T_{pi}$ and moves to the top of the wafer holder at $t = 80T_{pi}$. The tiny small squares observed in Fig. 3(b) at $t = 5T_{pi}$ and $t = 80T_{pi}$ are produced by a few ions (particles) escaping to that position.

The regional electric field for case three influences the ions differently as shown in Fig. 3(c). At $t = 5T_{pi}$, the regional

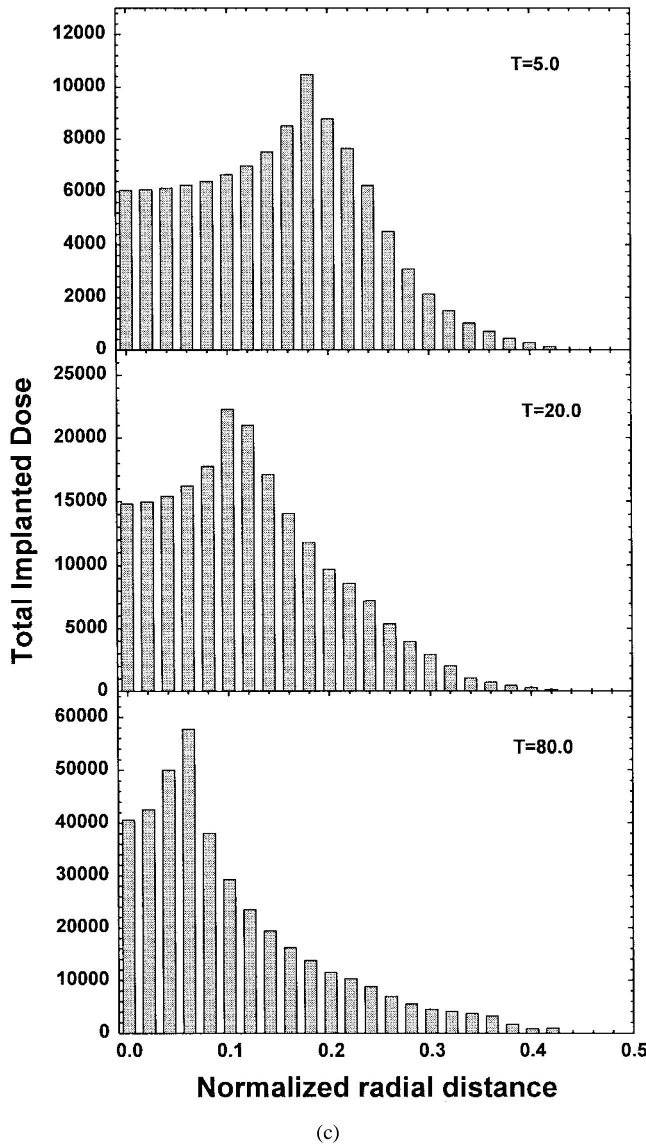

(c)

Fig. 5. *(Continued.)* (c) Variation of normalized total implantation dose along the surface of the wafer chuck at different times for case 3 [Fig. 1(c)]. Ions are implanted quite unevenly across the wafer.

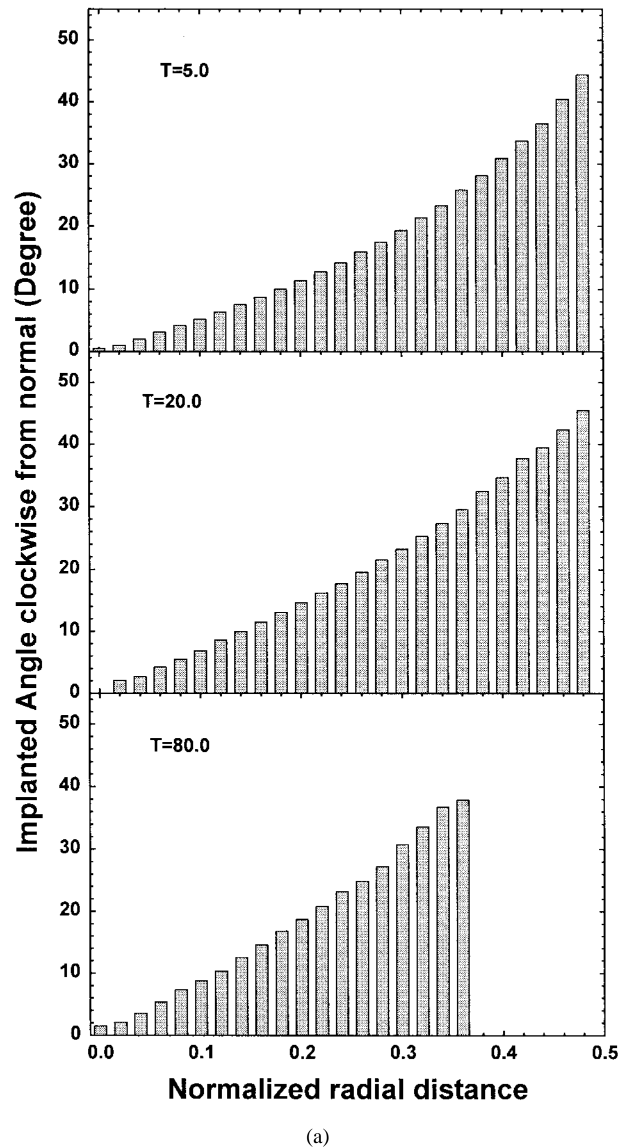

(a)

Fig. 6. (a) Variation of impact angle of ions along the surface of the wafer chuck at different times for case 1 [Fig. 1(a)].

electric field forces the ions to the center of the wafer holder creating an empty hole on top of the wafer holder. However, at $t = 20T_{pi}$ and $t = 80T_{pi}$, the empty hole is filled by a few ions (particles). These ions come from the other side of the symmetry boundary $\rho = 0$ (see ion velocity). A major portion of the ions are pushed toward the center and the zero ion density contour line is formed after $t = 80T_{pi}$.

C. Ion Velocity

The temporal evolution of the ion velocity vector is displayed in Fig. 4(a)–(i). The ion velocity vector for case one is shown in Fig. 4(a)–(c). The flow direction of the ions follows the square shape of the wafer holder. The flow direction does not change very much as the zero ion density contour line moves to the top of the wafer holder at $t = 80T_{pi}$ as shown in Fig. 4(a)–(c). Fig. 4(d)–(f) depicts the effect of the regional electric field formed at the right bottom part of the corner for case two. At $t = 5T_{pi}$ in Fig. 4(d) and $t = 20T_{pi}$ in Fig. 4(e), the ions near the corner are tilted counter clockwise toward the top left part of the corner creating a concentration of ions in that region. At $t = 80T_{pi}$ in Fig. 4(f), the zero ion density contour line has moved to the top of the wafer holder, and the influence of the regional electric field is consequently less.

Fig. 4(g)–(i) shows a different effect of the regional electric field formed at the top left part of the corner for case three. At $t = 5T_{pi}$ in Fig. 4(g), the ions at the top of the wafer holder are also tilted counter clockwise, but they flow toward the center of the wafer holder. At $t = 20T_{pi}$ in Fig. 4(h), the ions filling up the empty hole have a positive radial velocity. They should not come from the simulation region. Due to the counter clockwise push, ions can gain a larger negative radial velocity and therefore a greater chance to cross the boundary ($\rho = 0$). Since equal number of ions from the other side of the boundary with opposite radial velocity will replace the lost ions, it is not surprising that ions with positive radial velocity

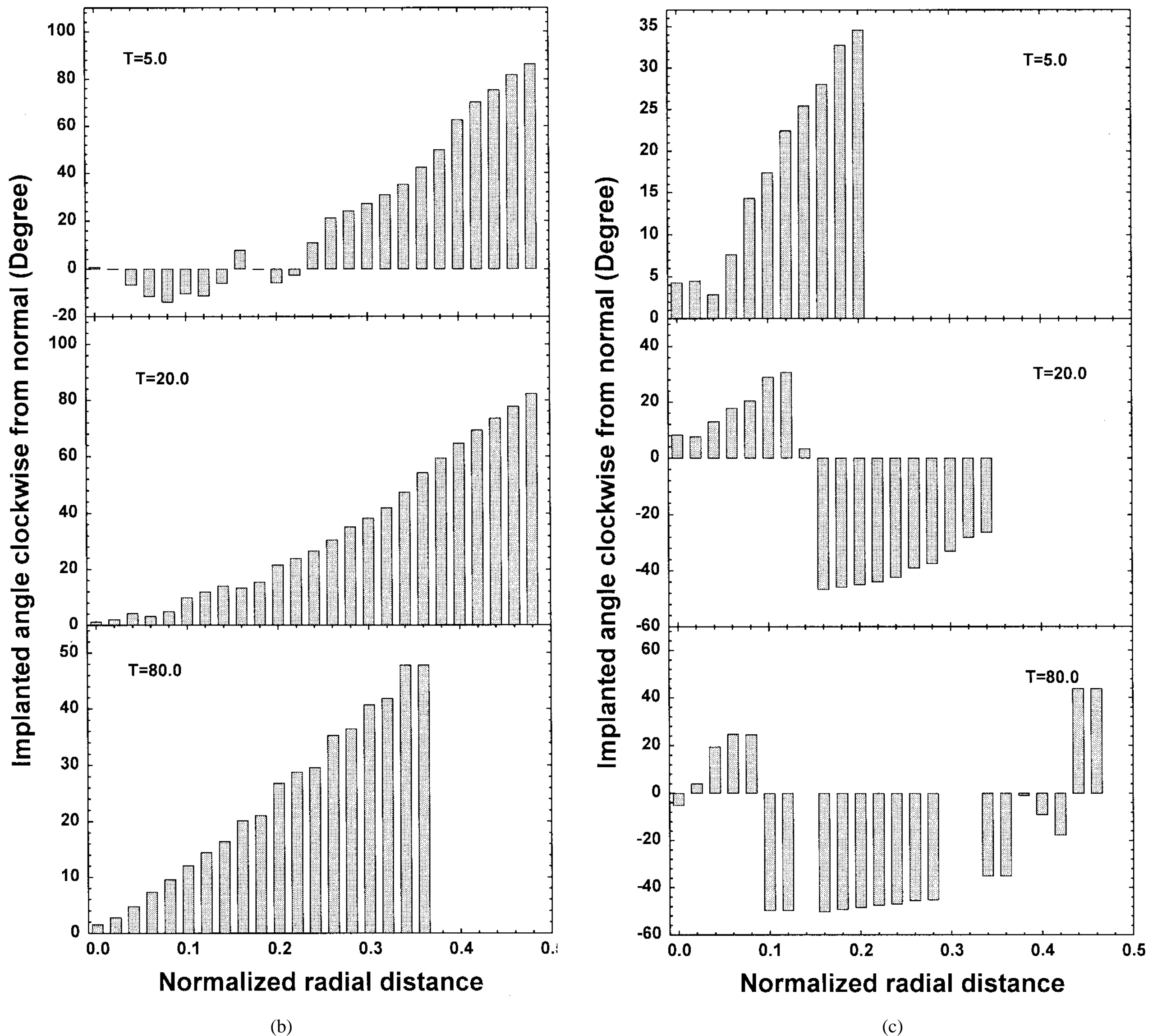

Fig. 6. *(Continued.)* (b) Variation of impact angle of ions along the surface of the wafer chuck at different times for case 2 [Fig. 1(b)]. (c) Variation of impact angle of ions along the surface of the wafer chuck at different times for case 3 [Fig. 1(c)].

are observed as our kinetic model allows particles (ions) to pass through each other.

D. Implantation Doses

The total implantation doses at different time $t = 5T_{pi}$, $20T_{pi}$, and $80T_{pi}$ are plotted in Fig. 5(a)–(c). Fig. 5(a) depicts the lateral ion dose variation in the wafer for case one. The difference between the center ($\rho = 0$) and the edge ($\rho = 0.5$) is relatively small at $t = 5T_{pi}$ and $20T_{pi}$. However, when the presheath hits the chamber sidewall and the zero ion density contour exists, the difference in doses between the center and the edge becomes larger at $t = 80T_{pi}$ since part the wafer holder surface is not implanted [see Fig. 3(a) at $t = 80T_{pi}$].

For case two, under the influence of the regional electric field, a sharp peak is observed at the edge as shown in Fig. 5(b) at $t = 5T_{pi}$ and $= 20T_{pi}$. A peak is formed because the electric field pushes the ions to that area the local implantation dose is higher. At $t = 80T_{pi}$, the sharp peak disappears since the effect of the regional electric field becomes negligible as the zero ion density contour line moves to the top surface of the wafer chuck. However, a drastic change in the implantation dose can be observed near $\rho = 0.4$.

The variation of the implantation dose at $t = 5T_{pi}$, $20T_{pi}$, and $80T_{pi}$ for case three is depicted in Fig. 5(c). It is apparent that the combined use of a quartz shroud and quartz plate provides the most uneven ion dose distribution. In fact, a sharp peak always exists and it shifts to the center of the wafer holder at $t = 80T_{pi}$.

E. Instant Impact Angle

The change of the ion impact angle along the surface of the wafer chuck is depicted in Fig. 6(a)–(c). The ion impact angle at $t = 5T_{pi}$, $20T_{pi}$, and $80T_{pi}$ for case one is displayed in Fig. 6(a). The impact angle is a consequence of the ion motion shown in Fig. 4(a). The ions are implanted into the wafer at a normal angle at the center but at more glancing angles near the edge.

The situation for case two is similar to that for case one as depicted in Fig. 6(b). At $t = 5T_{pi}$, some of the ions from the

other side of the boundary ($\rho = 0$) are implanted into the center region resulting in a slightly offset of impact angle. Due to the influence of the regional electric field, the ions are implanted almost horizontally near the corner of the wafer holder.

As shown in Fig. 4(g)–(i), the ion motion of case three is quite complicated. The regional electric field tilts the ions in a counter-clockwise direction and an empty area is formed on top of the wafer holder at $t = 5T_{pi}$. Therefore, the ions are implanted into the wafer holder at a larger impact angle as shown in Fig. 6(c). At $t = 20T_{pi}$ and $80T_{pi}$, a few ions come from the other side of the boundary covering the empty area. Hence, the ions are implanted the surface of the wafer holder at "positive" and "negative" impact angles [Fig. 6(c)].

V. Conclusion

Our simulation does not consider the steady-state Child–Langmuir sheath because in most high voltage and long pulse applications, for example, SOI formation, the size of the ion-matrix sheath is comparable to that of the plasma chamber. In such cases, all the ions will be implanted into the wafer chuck and no steady state will occur. Since the plasma source is usually placed on top of the chamber, the ions may not diffuse evenly to all parts of the chamber, especially the volume surrounding the wafer holder. In this situation, a steady-state sheath will occur but the shape is not easily defined. To simulate the steady-state conditions, the supply rate of plasma, flowing direction, and flowing rate of ions inside the chamber must be considered.

The use of quartz covers can reduce implantation into the wafer chuck and current drawn on the high voltage modulator. However, dose uniformity is severely compromised. Our results indicate that a plain wafer holder will yield the most uniform ion dose distribution across the wafer. The use of a quartz tube like the one in case two will concentrate the ions around the edge of the wafer chuck. The worst situation is to cover the outer region of the wafer holder by a quartz plate in addition to a quartz shroud.

The radius of the chamber is three times greater than the radius of the wafer holder in the simulation. This is a typical dimension in many PIII apparatus. As shown in Fig. 2(a), the presheath will hit the chamber in a very short period after the ion matrix has been established. It is also shown that the ions will exhaust and a zero ion density contour line will form [Fig. 3(a)]. At a later time, the zero ion density contour line moves to the top of the wafer holder leaving a sharp change in the implantation dose shown in Fig. 5(a). Therefore, a shorter pulse width will preclude the presheath from reaching the sidewall of the chamber and provide a more uniform implantation dose along the wafer surfaces. Ultimately, if long pulses are required, a bigger vacuum chamber is the preferred solution as a higher plasma density may violate the collisionless conditions required for mono-energetic implantation.

References

[1] P. K. Chu, S. Qin, C. Chan, N. W. Cheung, and L. A. Larson, "Plasma immersion ion implantation—A fledgling technique for semiconductor processing," *Mat. Sci. Engineering: Reports,* vol. R17, no. 6/7, pp. 207–280, 1996.

[2] N. W. Cheung, "Plasma immersion ion implantation for semiconductor processing," *Mat. Chem. Phys.,* vol. 46, pp. 132–139, 1996.

[3] P. K. Chu, N. W. Cheung, and C. Chan, "Recent applications of plasma immersion ion implantation," *Semicond. Int.,* vol. 6, pp. 165–172, June 1996.

[4] J. V. Mantese, I. G. Brown, N. W. Cheung, and G. A. Collins, "Plasma-immersion ion implantation," *MRS Bulletin,* vol. 21, no. 8, pp. 52–56, 1996.

[5] T. Sheng, S. B. Felch, and C. B. Cooper, "Characteristics of a plasma doping system for semiconductor device fabrication," *J. Vac. Sci. Technol. B,* vol. 12, no. 2, pp. 969–972, 1994.

[6] B. Mizuno, H. Nakaoka, M. Takase, A. Hori, I. Nakayama, and M. Ogura, "New methods for ultra-shallow Boron doping by using plasma, plasma-less and sputtering," in *Extended Abstracts 1995 Int. Conf. Solid State Devices Mat.,* Osaka, Japan, 1995, pp. 1041–1042.

[7] B. Mizuno, M. Takase, I. Nakayama, and M. Ogura, "Plasma doping and plasma-less doping of silicon," in *Symp. VLSI Tech. Dig.,* Honolulu, HI, 1996, p. 66.

[8] S. Qin and C. Chan, "Plasma immersion ion implantation doping experiments for microelectronics," *J. Vac. Sci. Technol. B,* vol. 12, no. 2, pp. 962–968, 1994.

[9] J. Min, P. K. Chu, Y. C. Cheng, J. B. Liu, S. Im, S. Iyer, and N. W. Cheung, "Buried oxide formation by plasma immersion ion implantation," *Mat. Chem. Phys.,* vol. 40, no. 3, pp. 219–222, 1995.

[10] J. B. Liu, S. S. K. Iyer, C. M. Hu, N. W. Cheung, R. Gronsky, J. Min, and P. Chu, "Formation of buried oxide in silicon using separation by plasma implantation of oxygen (SPIMOX)," *App. Phys. Lett.,* vol. 67, no. 16, pp. 2361–2363, 1995.

[11] J. Min, P. K. Chu, Y. C. Cheng, J. Liu, S. S. Iyer, and N. W. Cheung, "Nucleation mechanism of SPIMOX (separation by plasma implantation of oxygen)," *Surf. Coatings Technol.,* vol. 85, no. 1/2, pp. 60–63, 1996.

[12] P. K. Chu, X. Lu, S. S. K. Iyer, and N. W. Cheung, "A new way to make SOI wafers," *Solid State Technol.,* vol. 40, no. 5, pp. S9–S14, 1997.

[13] X. Lu, S. S. K. Iyer, J. B. Liu, C. M. Hu, N. W. Cheung, J. Min, and P. K. Chu, "Separation by plasma implantation of oxygen to form silicon on insulator," *Appl. Phys. Lett.,* vol. 70, no. 13, pp. 1748–1750, 1997.

[14] S. S. K. Iyer, X. Lu, J. B. Liu, J. Min, Z. Fan, P. Chu, C. M. Hu, and N. W. Cheung, "Separation by plasma implantation of oxygen (SPIMOX) operational phase space," *IEEE Trans. Plasma Sci.,* vol. 25, pp. 1128–1135, Oct. 1997.

[15] X. Lu, N. W. Cheung, M. D. Strathman, P. K. Chu, and B. Doyle, "Hydrogen induced silicon surface layer cleavage," *Appl. Phys. Lett.,* vol. 71, no. 13, pp. 1804–1806, 1997.

[16] X. Lu, S. S. K. Iyer, C. M. Hu, N. W. Cheung, J. Min, Z. N. Fan, and P. K. Chu, "Ion-cut silicon-on-insulator fabrication with plasma immersion ion implantation," *Appl. Phys. Lett.,* vol. 71, no. 19, pp. 2767–2269, 1997.

[17] P. K. Chu, S. Qin, C. Chan, N. W. Cheung, and P. K. Ko, "Instrumental and process considerations for the fabrication of silicon-on-insulator (SOI) structures by plasma immersion ion implantation," *IEEE Trans. Plasma Sci.,* vol. 26, pp. 79–84, Feb. 1998.

[18] J. D. Bernstein, S. Qin, C. Chan, and T. J. King, "Hydrogenation of polycrystalline silicon thin film transistors by plasma ion implantation," *IEEE Electron Device Lett.,* vol. 16, no. 10, pp. 421–423, 1995.

[19] Z. Fan, P. K. Chu, C. Chan, and N. W. Cheung, "Sample stage induced dose and energy nonuniformity during plasma immersion on implantation," *Appl. Phys. Lett.,* vol. 73, no. 2, pp. 202–204, 1998.

[20] J. R. Conrad, J. L. Radtke, R. A. Dodd, F. J. Worzala, and N. C. Tran, "Plasma source ion implantation technique for surface modification of materials," *J. Appl. Phys.,* vol. 62, no. 11, pp. 4591–4596, 1987.

Dixon Tat-Kun Kwok, for a photograph and biography, see p. 180 of the April 1998 issue of this Transactions.

Paul K. Chu (M'97), for a photograph and biography, see p. 180 of the April 1998 issue of this Transactions.

Chung Chan (S'79–M'81–SM'88–F'97), for photograph and biography, see this issue, p. 1590.